High temperature Mössbauer effect study of $Fe_{90}Zr_7B_3$ nanocrystalline alloy

2005 J. Phys.: Condens. Matter 17 3183

(http://iopscience.iop.org/0953-8984/17/21/013)

INSTITUTE OF PHYSICS PUBLISHING JOURNAL OF PHYSICS: CONDENSED MATTER

J. Phys.: Condens. Matter **17** (2005) 3183–3196 doi:10.1088/0953-8984/17/21/013

High temperature Mössbauer effect study of $Fe_{90}Zr_7B_3$ nanocrystalline alloy

Svetoslav Stankov[1,2], Bogdan Sepiol[1], Tomáš Kaňuch[3], Dietmar Scherjau[4], Roland Würschum[4] and Marcel Miglierini[3]

[1] Institut für Materialphysik, Universität Wien, Strudlhofgasse 4, 1090 Wien, Austria
[2] European Synchrotron Radiation Facility, 6 rue Jules Horowitz, 38043 Grenoble, France
[3] Department of Nuclear Physics and Technology, Slovak University of Technology, Ilkovičova 3, 81219 Bratislava, Slovakia
[4] Technische Universität Graz, Petersgasse 16, 8010 Graz, Austria

Received 11 March 2005, in final form 7 April 2005
Published 13 May 2005
Online at stacks.iop.org/JPhysCM/17/3183

Abstract

$Fe_{90}Zr_7B_3$ NANOPERM alloy is investigated in as-quenched and nanocrystalline forms by means of high temperature (up to 1040 K) Mössbauer spectroscopy. These studies are aimed at revealing the relationship of microstructure to magnetic properties for ^{57}Fe phases and their temperature dependences in NANOPERM-type ternary alloy at temperatures exceeding the onset of the second crystallization. For this purpose the nanocrystalline sample was prepared by annealing an amorphous precursor at 893 K for 1 h providing 54% of bcc α-Fe nanocrystalline grains. At this stage the first crystallization is almost completed. Because of the progress of the crystallization process during the acquisition of Mössbauer spectra beyond the temperature of the first crystallization, the results obtained are discussed for three temperature intervals: below the first crystallization (782 K), between the first and the second crystallization, and above the second crystallization temperature (931 K). Conclusions related to the evolution of the crystalline fraction, interfacial regions and the amorphous residual phase are derived by comparing spectral parameters obtained from the *in situ* high temperature Mössbauer effect measurements with those from room temperature Mössbauer spectra acquired immediately after each high temperature experiment. The latter revealed structural modifications imposed during Mössbauer spectroscopy at high temperatures, whereas the *in situ* experiments identify thermally induced dynamic processes.

(Some figures in this article are in colour only in the electronic version)

1. Introduction

Since their discovery by Suzuki *et al* [1], NANOPERM nanocrystalline alloys have attracted a lot of attention mainly due to their excellent soft magnetic properties [2] that make them

suitable candidates for many practical applications [3]. These materials are also at the centre of research interest aimed at understanding their unique magnetic properties and in particular their relations with microstructural arrangement as well as their demonstration of macroscopic physical properties. Even though a great deal of investigation of Fe–Zr–B nanocrystalline alloys has been performed, new approaches are still looked for, to elucidate the processes which are taking place during the crystallization. Nagase *et al* [4] reported accelerated crystallization and changes in phase stability caused by electron irradiation of $Fe_{88}Zr_9B_3$ and $Fe_{71}Zr_9B_{20}$ amorphous alloys. On the basis of experimental observations, the crystallization kinetics and chemical partitioning during crystallization of FINEMET, NANOPERM and HITPERM, with general formulae FeSiBNbCu, FeMBCu and $(Fe_{1-x}Co_x)_{88}M_7B_4Cu$, respectively, with M = Nb, Zr, Hf, nanocrystalline alloys were theoretically treated by McHenry *et al* [5]. The relation between magnetism and structure was investigated by Kopcewicz *et al* [6] in a NANOPERM-like $Fe_{(81-x)}Ni_xZr_7B_{12}$ system by a detailed study of the crystallization process employing conventional Mössbauer spectroscopy performed at 80 and 300 K, conversion electron Mössbauer spectroscopy as well as an unconventional radio-frequency Mössbauer technique.

Questions related to the microstructure–magnetic properties relationship are still open because of the complexity of the problem. Possibilities of controlling soft magnetic properties were discussed by Gao *et al* [7] for $Fe_{90}Zr_7B_3$ nanocrystalline alloy employing *in situ* Lorentz microscopy for observations of domain walls. It was shown that a two-step annealing can remove internal stresses thus optimizing the microstructure situation. Recent x-ray diffraction studies of the same ternary alloy reveal microstrains in the region of 0.12% as determined by Hall analysis [8]. Mössbauer spectroscopy was used by Yoon *et al* [9] to investigate by means of hyperfine parameters crystallographic changes induced during the annealing of $Fe_{83}B_9Nb_7Cu_1$ alloy. Special attention was paid to the structure of interface regions located between the nanocrystalline and amorphous matrices. The effects of modification of the chemistry of the residual amorphous phase on soft magnetic and magnetotransport properties of nanocrystalline $Fe_{(89-x)}Zr_7B_3Cu_1Ge_x$ and $Fe_{(91-x)}Zr_8Cu_1Ru_x$ alloys were reported by Suzuki *et al* [10, 11] using also room temperature Mössbauer spectroscopy.

For closer inspection of the behaviour of hyperfine interactions temperature dependences of Mössbauer spectral parameters should be examined. Nevertheless, there are only few works in the literature devoted to NANOPERM-type alloys studied at elevated temperatures. The interfaces formed at crystalline grain–amorphous matrix boundaries were shown to exhibit temperature dependences of the hyperfine fields similar to that of body centred cubic (bcc) α-Fe phase for $Fe_{89}Zr_7B_4$ nanocrystalline alloy in the range from 4.2 up to 550 K [12]. Changes in microstructure, crystallization behaviour and magnetic states of $Fe_{(87.5-x)}Cu_xZr_{6.5}B_6$ alloys with different contents of nanograins were examined in temperature range 77–473 K [13]. The results obtained supported theoretical predictions concerning the propagation of ferromagnetic exchange interactions between the nanograins through the amorphous matrix and indicated the significant role played by interfacial regions. Similar results were reported also for $Fe_{91}Zr_7B_2$ [14], $Fe_{87.5}Zr_{6.5}B_6$ [15], but also for $Fe_{80}Nb_7B_{12}Cu_1$ [16], $Fe_{86-x}Cu_1Nb_xB_{13}$ [17] and for $Fe_{80}M_7Cu_1B_{12}$ (M = Mo, Nb, Ti) [18] nanocrystalline alloys.

The effect of concentration fluctuations is emphasized [19], to explain the apparent smearing of the Curie temperature in nanocrystalline $Fe_{80}Zr_7B_{12}Cu_1$ alloy. The temperature evolution of hyperfine fields of bcc Fe nanocrystals formed in $Fe_{(92-x)}Zr_7B_xCu_1$ alloys [20, 21] is explained by impurities contained in the bcc phase, which are supposed to have a dominant influence on the advantageous soft magnetic properties. A small percentage (about 4%) of Fe sites which cannot be assigned either to the bcc or to the residual amorphous phase are detected but the presence of interfacial regions is questioned [21]. On the other hand,

experimental evidence from Mössbauer investigations performed over a wide temperature range and supported by the results from atom probe field ion microscopy, EXAFS and FMR analysis are in favour of the existence of the interface zone with a thickness of about 2–3 atomic layers [22].

As we demonstrated above, the vast majority of works performed upon the Fe–Zr–B system were engaged in elucidation of the structure to magnetic microstructure relationship. Mössbauer effect experiments were usually carried out at temperatures below the temperature of the onset of the first crystallization for the particular sample composition. In this paper, we present the results of Mössbauer investigations carried out on $Fe_{90}Zr_7B_3$ nanocrystalline alloy at temperatures that eventually extend behind the second crystallization stage. *In situ* high temperature studies and subsequent room temperature verification measurements are aimed at revealing the microstructure to magnetic properties relation and the temperature dependence of each ^{57}Fe-containing structural phase present in the nanocrystalline sample.

2. Experimental details

Amorphous $Fe_{90}Zr_7B_3$ ribbon with 21(1) μm thickness and 15 mm width was prepared by the melt-spinning technique in a protective atmosphere. The amorphous state of the starting material was evidenced by Mössbauer spectroscopy at room temperature (RT). The nanocrystalline structure has been produced by annealing the amorphous ribbon at 893 K for 1 h under high vacuum conditions. Transmission Mössbauer spectroscopy was employed using a ^{57}Co(Rh) source with about 20 mCi activity. A conventional spectrometer working in constant acceleration mode and a proportional counter have been applied to study the $Fe_{90}Zr_7B_3$ alloy *in situ*. A home made resistance heating furnace with Kapton windows, beryllium heat shielding and water cooling has been used for high temperature (HT) Mössbauer measurements. Mössbauer spectra were recorded at different temperatures in the interval between 77 and 1040 K. After every HT spectrum the sample was cooled and the following RT spectrum was collected in order to monitor the state of the sample. All spectra were recorded with the sample placed inside the furnace, thus ensuring the same geometrical conditions for both HT and RT Mössbauer experiments. The mean time duration of each measurement was about 7(1) hours.

All isomer shift (IS) values are quoted with respect to the room temperature Mössbauer spectrum of a 20(1) μm thick α-Fe calibration foil.

Crystallization temperatures of the $Fe_{90}Zr_7B_3$ alloy were detected by differential scanning calorimetry (DSC) using a Perkin-Elmer DSC 7 instrument with a heating rate of 10 K min^{-1}.

3. Fitting model applied to Mössbauer spectra

Choosing a fitting model for the Mössbauer spectra of NANOPERM-type alloys is not straightforward. To refine the spectral parameters, a variety of approaches have been introduced [13, 14, 17, 20, 23–27]. In general, all of them agree on the presence of three different spectral components but offer apparently different interpretations.

Figure 1(a) shows the Mössbauer spectrum of the nanocrystalline sample investigated, taken at RT before HT measurements. The well pronounced narrow sextet (solid line component) originates from the nanocrystalline phase (CR) formed in the sample upon annealing. As derived from a variety of experimental techniques, in Si-free NANOPERM alloys the nanocrystalline fraction is represented by the bcc phase of α-Fe [2, 28–30]. The hyperfine parameters of the solid line component obtained from our fit to the experimental

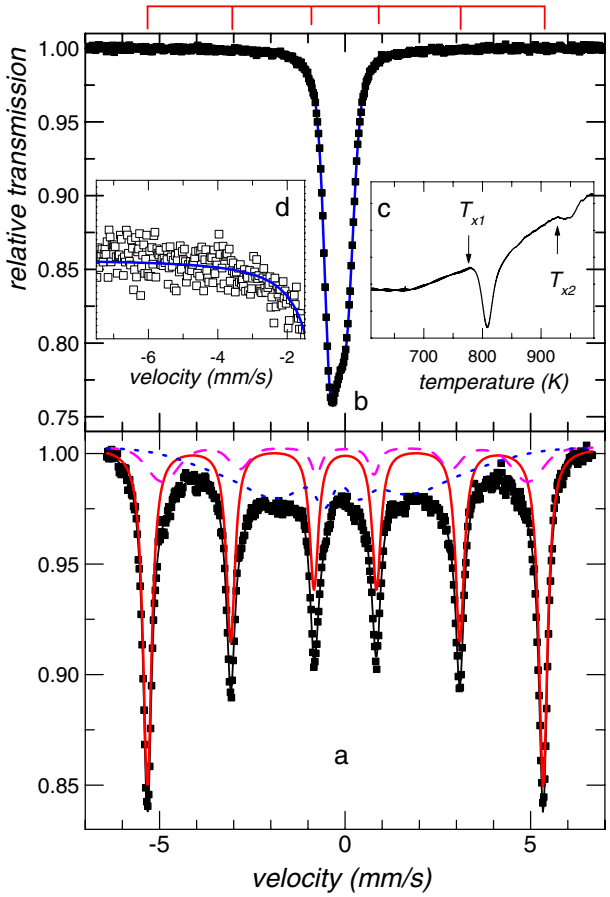

Figure 1. Room temperature Mössbauer spectra of $Fe_{90}Zr_7B_3$ alloy: (a) after annealing at 893 K for 1 h and (b) in the amorphous as-cast state. Spectral components in (a) represent the crystalline phase CR (solid line), interface regions IF (dashed line) and amorphous residual matrix AM (dotted line). (c) shows a DSC scan performed upon the amorphous sample. The onsets of the first T_{x1} and the second T_{x2} crystallizations are marked with arrows. (d) represents the magnified spectral region between -7 and -2 mm s^{-1} from the Mössbauer spectrum shown in (b) (see section 4 for details).

Mössbauer spectrum in figure 1(a) yield values of magnetic field $B_{CR} = 33.05(5)$ T and isomer shift $IS_{CR} = 0.005(2)$ mm s^{-1} that confirm the formation of α-Fe nanocrystallites.

The broad component in the Mössbauer spectrum plotted as the dotted line in figure 1(a) is ascribed to Fe atoms located in the residual amorphous matrix (AM). The non-homogeneous surroundings of these atoms (distribution in the coordination number of Fe atoms) imply a distribution in magnetic fields experienced by the resonant nuclei. Therefore this subspectrum is fitted by distributions of both the magnetic field and the isomer shift with a correlation parameter connecting them. The corresponding mean values obtained from the fit are $\langle B_{AM}\rangle = 16(1)$ T and $\langle IS_{AM}\rangle = 0.12(4)$ mm s^{-1}. Eventually, distributions related to paramagnetic and ferromagnetic regions in the amorphous retained phase are employed, especially at elevated temperatures, i.e. in the vicinity of Curie transition of the AM phase.

The third component, plotted in figure 1(a) as a dashed line, is assigned to Fe atoms located in interface regions between the nanograins and the residual amorphous material. Two

types of atom can be distinguished in this area: (i) Fe atoms located at the nanocrystalline surfaces; and (ii) Fe atoms which still belong to the amorphous phase but have in the first coordination sphere atoms from the nanograin surfaces (type (i)) [17, 23, 26, 27]. Both types of atom are referred to as interface components (IF). Due to the non-equivalent and not well defined first and second coordination spheres these atoms experience a different, slightly decreased magnetic field compared to those located inside the bcc lattice. Therefore the intermediate broad sextet (dashed line component) is fitted with a distribution of the magnetic field resulting in the mean value $\langle B_{\mathrm{IF}} \rangle = 29.9(5)$ T which is about 3 T lower than that of the CR phase.

All Mössbauer spectra presented in this paper are fitted with the 'Recoil' Mössbauer spectral analysing software using the extended Voigt-based fitting model [31, 32]. The main restrictions implied in this model are: (a) that the quadrupole splitting ΔE_{Q} is much smaller than the magnetic splitting for the magnetic subsites (first-order perturbation approximation); and (b) that the hyperfine interactions are effectively static. The first condition is well fulfilled since the Mössbauer spectra are symmetric with respect to their centre of gravity. However, additional fits with ΔE_{Q} being a fit parameter have been performed, the result of which was always zero in the experimental error range, showing that the first-order perturbation approximation holds.

The second restriction is related to the possible presence of relaxation effects at elevated temperatures. Superparamagnetic relaxation has been observed in nanocrystalline $Fe_{80}Zr_7B_{12}Cu_1$ alloy with average grain sizes of about 8–10 nm at temperatures up to 900 K, but it has not been detected in $Fe_{90}Zr_7B_2Cu_1$ having nanograin sizes of the same order of magnitude [19]. The initial annealing of our sample at 893 K for 1 h results in well developed nanocrystalline structure with an average grain size of about 20 nm (see section 4). Even at the highest measuring temperature the Lorentzian profile with a linewidth of about 0.39(1) mm s^{-1} satisfactorily describes the line shape of the CR subspectrum. Therefore we exclude the possibility of the presence of any remarkable superferromagnetic relaxation effects in the sample under investigation and thus both conditions implied by the model are well fulfilled.

4. Results

Figure 1(b) shows the Mössbauer spectrum of the amorphous as-cast $Fe_{90}Zr_7B_3$ alloy measured at RT before annealing of the sample in order to show the amorphous nature of the ribbon produced. Ambiguous results can be found in the literature concerning the precipitation of α-Fe nanocrystallites already in the original as-cast material. Transmission electron microscopy (TEM) does not show the presence of any crystalline structure in the amorphous specimen [29, 33] whereas high resolution electron microscopy (HREM) investigations confirm the precipitation of bcc Fe clusters with dimensions as small as 1 nm [30, 34]. In order to detect nanocrystallites possibly present in the amorphous ribbon with reliable precision the Mössbauer spectrum has been recorded with high statistics. The lines above the spectrum shown in figure 1(b) mark the positions of the sextet corresponding to α-Fe bcc phase. Since the first and the sixth line have the highest intensity, traces of nanocrystalline precipitates, if any are present in the sample, have to be visible at these velocities. Our simulations have shown that the CR phase in this spectrum can be reliably detected if the corresponding relative area exceeds 0.8% of all ^{57}Fe atoms. Figure 1(d) shows a magnified part of the spectrum of the amorphous alloy in the velocity range between -7 and -2 mm s^{-1}, from which one cannot deduce the presence of nanocrystallites. Therefore from the Mössbauer spectrum shown in figures 1(b) and (d) we can exclude the possibility of the formation of α-Fe nanoclusters which contain more than 1% of the resonant atoms in the sample.

Mössbauer and x-ray diffraction (XRD) investigations of the crystallization kinetics of this particular ternary alloy revealed that the nucleation and grain growth are quite fast processes [37]. According to these studies, after annealing the amorphous ribbon for about 10 min at 798 K (slightly above the first crystallization temperature of 782 K) the processes of nucleation and grain growth are already completed. In order to investigate the high temperature behaviour of the hyperfine parameters of all subsites present in the sample the amorphous ribbon was annealed at 893 K for 1 h. This treatment produces well developed nanocrystalline structure with average grain size of about 20 nm as obtained from combined XRD and HREM investigations [8].

The Mössbauer spectrum of the nanocrystalline $Fe_{90}Zr_7B_3$ alloy measured at RT before the HT experiments is shown in figure 1(a). According to the fitting model described in section 3, about 33% of Fe atoms are located in the amorphous matrix, 13% in the interface regions and the remaining 54% form α-Fe nanograins. These values are in excellent agreement with those obtained from XRD giving about 34% of AM [8] and from Mössbauer and XRD studies performed on the same type of nanocrystalline alloy [35].

Figure 2 shows typical Mössbauer spectra of the nanocrystalline $Fe_{90}Zr_7B_3$ alloy taken at the temperatures indicated. The spectral components represent the CR (solid line), IF (dashed line) and AM (dotted line) phases. Please note that in figures 2(a) and (b) two dotted line subspectra are present, which results from a coexistence of magnetically ordered and paramagnetic states of the Fe atoms in the AM phase. Values of the hyperfine magnetic field B_f, isomer shift IS_f and relative area A_f (f = AM, CR, IF) as derived from the fit to the Mössbauer spectra are plotted in figure 3 against the temperature of measurement T_{mes}. For comparison, temperature dependences of B_{hf} and IS obtained from Mössbauer spectra of the calibration α-Fe foil are also shown in figures 3(a) and (b), respectively.

Immediately after each Mössbauer experiment, performed at various temperatures T_{mes} the sample was cooled and room temperature spectra were collected. Some of them are displayed in figure 4 together with their subspectral components representing the CR (solid line), IF (dashed line) and AM (dotted line) phases. The hyperfine magnetic field B_f, isomer shift IS_f and relative area A_f (f = AM, CR, IF) as obtained from room temperature Mössbauer spectra are plotted in figures 5(a), (b) and (c) respectively, against the temperature at which the original HT experiments were performed. It should be noted that the abscissa in figure 5 is the same as that in figure 3 but here it represents the temperatures of the preceding HT measurements rather then the temperature itself.

5. Discussion

It is well known that the crystallization of Fe-based metallic glasses is a two-step process [36]. The primary crystallization leads to precipitation of nanocrystalline phase, bcc α-Fe in Si-free NANOPERM-type alloys in the residual amorphous matrix. Above the second crystallization temperature the residual amorphous matrix forms secondary crystalline phases [29]. The differential calorimetric scan shown in figure 1(c), for the amorphous $Fe_{90}Zr_7B_3$ ribbon, determines the onsets of the first and the second crystallizations to be at $T_{x1} = 782$ K and $T_{x2} = 931$ K, respectively. Accounting for these values we divide up the discussion of the high temperature Mössbauer studies accordingly to cover the following three temperature intervals: from RT to T_{x1}; between T_{x1} and T_{x2}; and above T_{x2}, marked with vertical dashed lines in figures 3 and 5.

5.1. Temperature measurements in the range RT–782 K

The temperature dependence of the hyperfine magnetic field obtained for the CR phase plotted in figure 3(a) is in very good agreement with already published data for this temperature

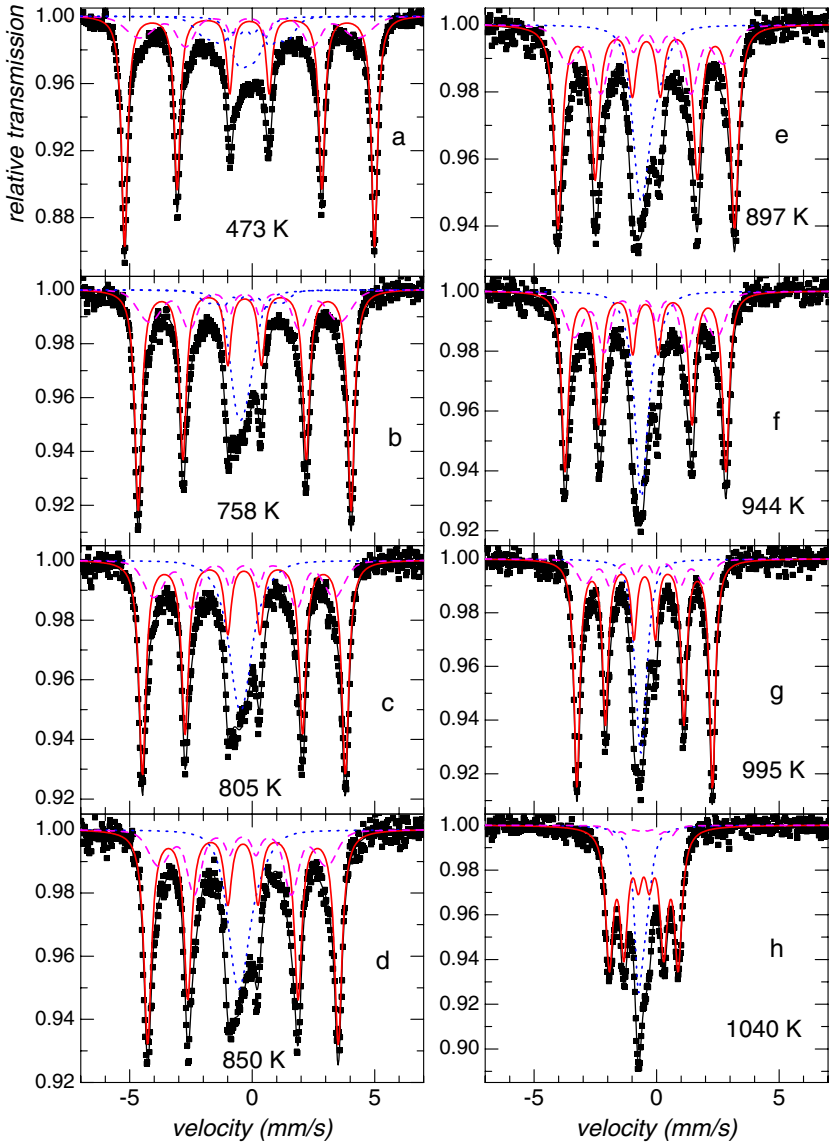

Figure 2. Mössbauer spectra of nanocrystalline $Fe_{90}Zr_7B_3$ alloy measured at the temperatures indicated. Spectral components represent the crystalline phase CR (solid line), interface regions IF (dashed line) and amorphous residual matrix AM (dotted line). Two dotted line components in the Mössbauer spectra shown in (a) and (b) result from a coexistence of magnetic and paramagnetic states of the Fe atoms in the AM phase.

range [21]. The temperature evolution of the hyperfine magnetic field of the IF component is shown in figure 3(a) as well. As can be seen, it follows closely that of the CR phase, exhibiting systematically lower values of the magnetic field. Such behaviour is experimentally observed in NANOPERM-type alloys and it is attributed to disordered surroundings of the Fe atoms and their neighbourhoods in the grain boundaries [13, 23]. It also indicates a close similarity of the nearest neighbourhood which belongs to the grains and interfacial regions [18].

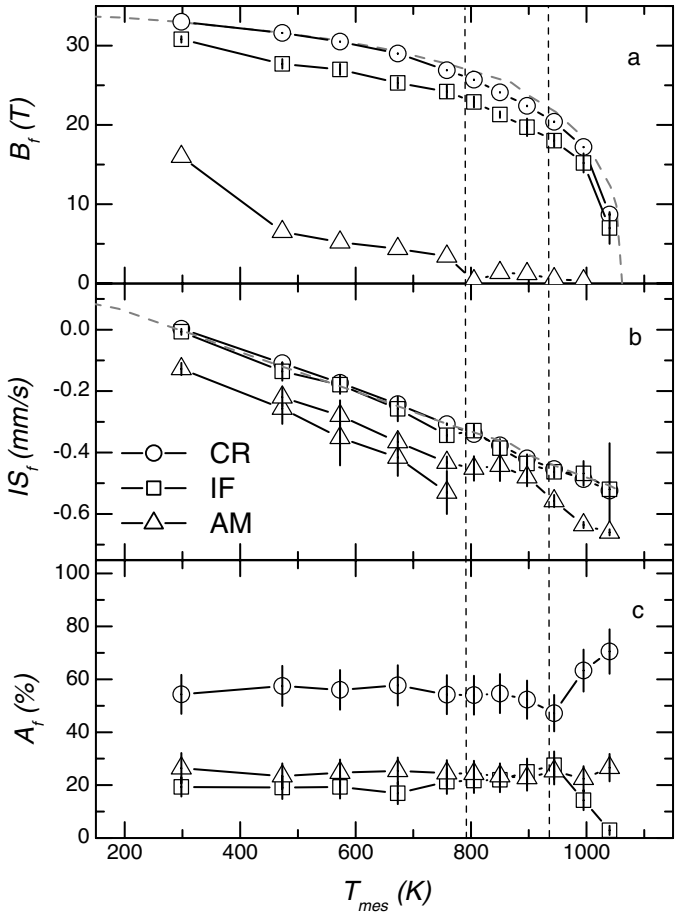

Figure 3. Hyperfine magnetic field B_f (a), isomer shift IS_f (b) and relative area A_f (c) as derived from high temperature Mössbauer spectra of nanocrystalline $Fe_{90}Zr_7B_3$ alloy plotted against the temperature of measurement T_{mes} for individual spectral components: $f = AM(\triangle)$, CR (○) and IF (□). Dashed grey lines in (a) and (b) represent B_{hf} and IS respectively for α-Fe foil. Vertical dashed lines mark first and second crystallization temperatures T_{x1} and T_{x2}.

Another interpretation of the IF spectral component assumes dissolved Zr and/or B atoms in the first or second coordination spheres of the resonant atoms, thus creating impurities located inside the bcc nanocrystalline lattice. A remarkable decrease in Curie temperature of the α-Fe nanocrystalline phase (observed however for NANOPERM alloys with higher content of B atoms) and slightly increased lattice parameter are interpreted as experimental evidence supporting this model (a detailed overview can be found in [21]).

In the experimental and theoretical works published up to now there are results supporting both models concerning the origin of the intermediate component in the Mössbauer spectra of NANOPERM-type alloys. Thought the possibility of the presence of a few impurity atoms inside the bcc lattice cannot be excluded, even 3–4% [21] would still not be enough to explain the reduction of the hyperfine field observed. Moreover, the contribution of the interface atoms to the overall spectrum cannot be neglected since the dimensions of the grains are in the nanoscale region where the impact of the surface of the grains becomes important. The presence of interface regions in this particular ternary alloy has been recently

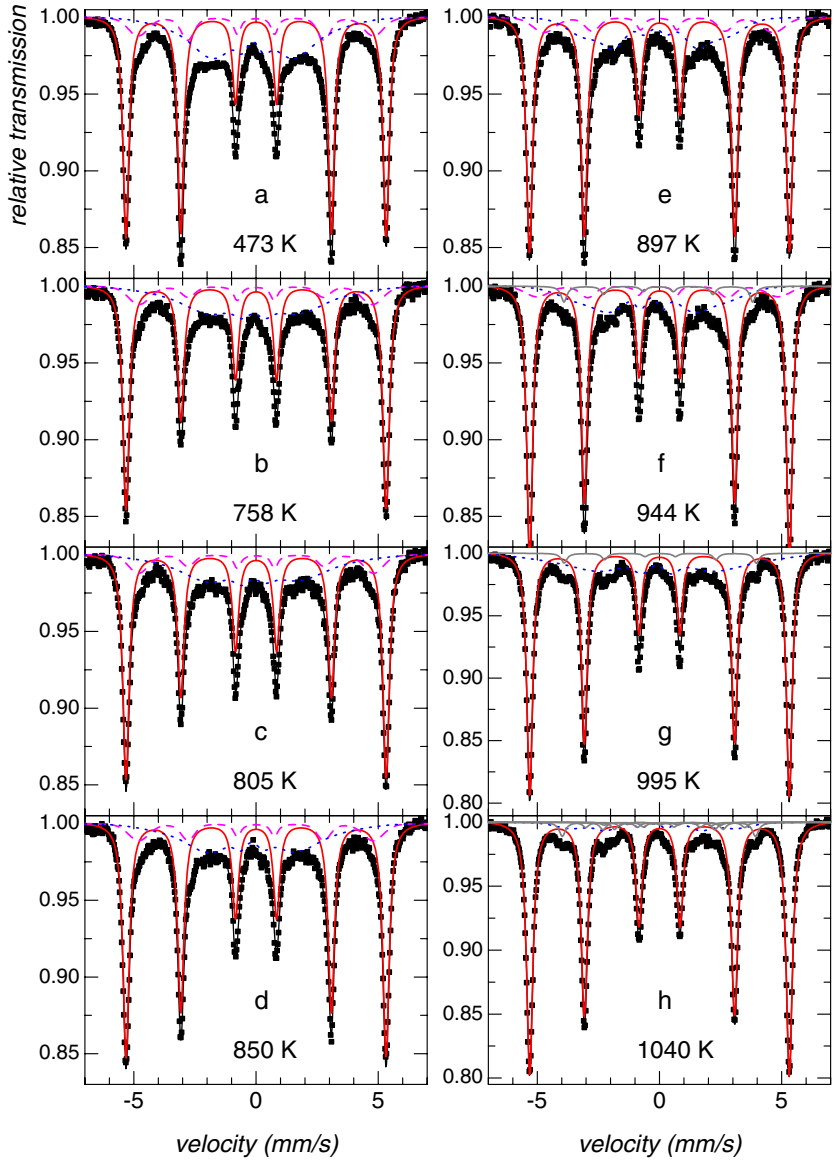

Figure 4. Mössbauer spectra of nanocrystalline $Fe_{90}Zr_7B_3$ alloy recorded at room temperature after measurements at the temperatures indicated. Spectral components represent the crystalline phase CR (solid line), interface regions IF (dashed line) and amorphous residual matrix AM (dotted line). A grey line in (f)–(h) represents the second crystalline phase.

evidenced by HREM and energy dispersive x-ray studies as well as by positron annihilation investigations [8]. The concept of an interfacial zone, resulting from the symmetry restriction at the periphery of the crystalline grains in the nanocrystalline alloys, is also discussed on the basis of Mössbauer investigations performed over a wide temperature range and the results obtained are in agreement with the atom probe field ion microscopy, EXAFS and FMR analysis [22].

The only process which can be observed in the HT Mössbauer spectra measured in this range is the magnetic to paramagnetic transformation (Curie transition) of the residual

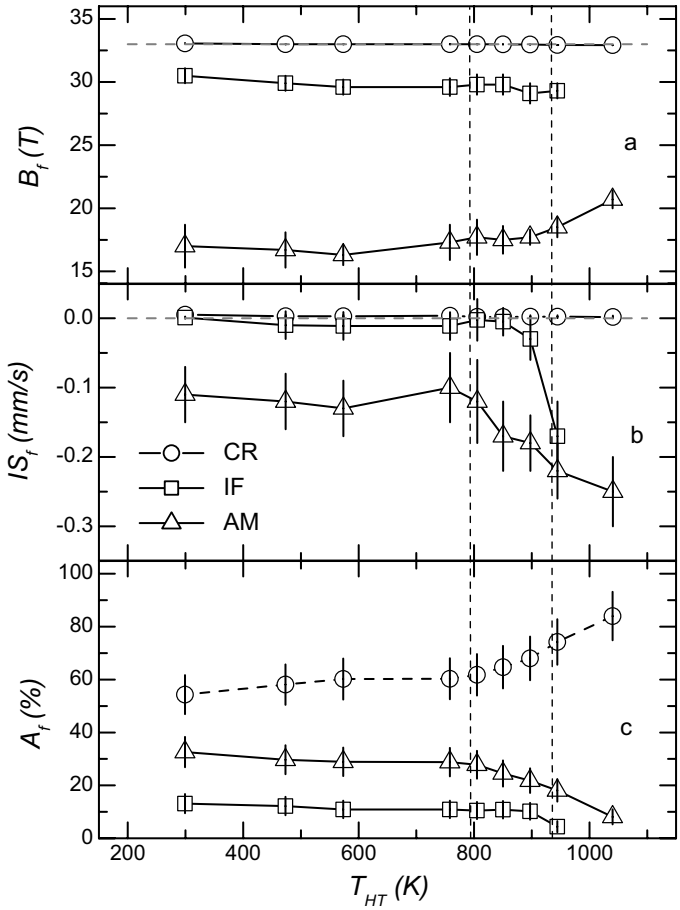

Figure 5. Hyperfine magnetic field B_f (a), isomer shift IS_f (b) and relative area A_f (c) as derived from room temperature Mössbauer spectra of nanocrystalline $Fe_{90}Zr_7B_3$ alloy plotted against the temperature T_{HT} at which the original HT experiments were performed for individual spectral components: $f = AM$ (△), CR (○) and IF (□). Room temperature values of $B_{\mathrm{hf}} = 33.0$ T and $\mathrm{IS} = 0.0$ mm s^{-1} for α-Fe foil are indicated by dashed grey lines in (a) and (b), respectively. Vertical dashed lines mark first and second crystallization temperatures T_{x1} and T_{x2}.

amorphous matrix. This transition starts at 473 K (figure 2(a)) and at 573 K (not shown in the figure) half of the iron atoms located in AM are already paramagnetic. Nevertheless, a small contribution of magnetic regions can still be detected even at 758 K (figure 2(b)). Consequently, the Curie temperature $T^{\mathrm{C}}_{\mathrm{AM}}$ of the retained amorphous phase is smeared out over a broad temperature range, which indicates that magnetically active and paramagnetic regions coexist. Taking into consideration that the as-cast amorphous sample is fully paramagnetic at room temperature (compare the Mössbauer spectra in figure 1) an enormous enhancement of $T^{\mathrm{C}}_{\mathrm{AM}}$ is observed. This increase in $T^{\mathrm{C}}_{\mathrm{AM}}$ during crystallization of NANOPERM-type alloys is attributed to two factors [37]: (i) compositional changes in the retained amorphous phase; and (ii) crystalline exchange field penetration. The latter is the dominating factor for samples with a large crystalline fraction which is indeed the case for the sample investigated.

The variation of the isomer shift with the measuring temperature for CR and IF components, shown in figure 3(b), coincides with that of α-Fe through all three temperature

intervals. Such temperature behaviour of the isomer shift strongly supports the assumption that Fe atoms of the IF component structurally belong to the CR surfaces. On the other hand, the presence of mainly Zr atoms (7% of the sample composition) in the residual amorphous matrix results in higher negative IS_{AM} values of this component. The upper and the lower curve correspond to paramagnetic and ferromagnetic regions inside the AM phase, respectively, which coexist in this temperature range. These values have not been fixed during the fitting procedure; nevertheless they coincide within the experimental error range.

5.2. Temperature measurements in the range 782–931 K

In order to prevent further crystallization of the sample investigated during measurements, the experiments are usually performed only up to the onset of the first crystallization or slightly above T_{x1}. Our investigations, extended well beyond T_{x1}, confirm that B_{CR} follows closely the temperature behaviour of the magnetic field in α-Fe foil (figure 3(a)). The observed deviation of less than 5 T is often attributed to the presence of few per cent of impurities inside the bcc lattice [21].

Figures 2(c)–(e) exhibit Mössbauer spectra of $Fe_{90}Zr_7B_3$ measured in the temperature interval between the first and the second crystallization stages. The relative area of the IF component, plotted in figure 3(c), increases from 17% below T_{x1} up to about 27%. An opposite effect is observed for A_{CR} while A_{AM} remains constant in this temperature interval. These tendencies are indications of a dynamic process, which takes place during the measurement associated with the crystallization, including also redistribution of the constituent elements. Consequently, each Mössbauer spectrum measured at temperatures higher than T_{x1} is a superposition of spectra corresponding to different crystallization stages of the sample. The Mössbauer parameters obtained from the fit are averaged over the time of measurement (about 7 h) due to the evolution of the structure under study which takes place in this temperature range. Nevertheless, the temperature behaviours of B_f and IS_f, plotted in figures 3(a) and (b), respectively, exhibit the same trends as discussed in the previous section. More reliable information about the structural changes which occur in this temperature interval can be deduced from RT Mössbauer spectra measured subsequently after each HT step, as discussed below.

5.3. Temperature measurements above 931 K

Remarkable changes take place in the sample on reaching the second crystallization temperature T_{x2}. Relative area values obtained from HT Mössbauer spectra (see figures 2(f)–(h)) reveal a rapid increase of the CR phase and decrease of the IF component as seen in figure 3(c). The same tendency is observed also in RT spectra taken after HT measurements. Pronounced enhancement of A_{CR} is related to progressive crystallization leaving behind regions depleted in iron in the amorphous phase retained. Short range order changes in the latter are taking place and they are evidenced by reduction of IS_{AM} values in figure 3(b). Simultaneous decrease in A_{IF}, which eventually leads to complete disappearance of this phase at temperatures above 1040 K, indicates that the crystallites formed are already polycrystals and their dimensions are no longer in the nanometre range.

The second process which takes place in the temperature range above T_{x2} is precipitation of secondary crystalline phases. Their presence is more clearly indicated in the succeeding RT Mössbauer spectra measured after HT measurements.

5.4. Room temperature measurements after HT experiments

No appreciable changes are observed in spectral parameters in the first temperature interval, i.e. from RT up to 782 K. The relative areas obtained from both HT (figure 3(c)) and RT

(figure 5(c)) Mössbauer spectra do not reveal redistribution of resonant atoms, which is expected since the first crystallization stage has not yet been reached. Looking at the Mössbauer spectra in figure 4 one can note deviations in the line intensities which are the most pronounced in figures 4(a) and (b). As the second and the fifth line intensities determine the orientation of the net magnetization of the sample they are affected by changes in the magnetic microstructure. The latter can be influenced by stresses generated during nanocrystallization which can be, consequently, annealed out during extended measurements at elevated temperatures.

In the second temperature interval (782–931 K), a relocation of resonant atoms from AM into CR is deduced from the decrease of A_{AM} accompanied by the simultaneous rise of A_{CR} as demonstrated in figure 5(c). This is caused by progress of the crystallization which, in this temperature interval, results in growth of the crystalline grains. A_{IF} remaining constant indicates that the crystallites are still of nanoscale dimensions.

A gain in A_{CR} of about 5% is found after the measurement at 850 K, which is still below the original annealing temperature (893 K). Thermal treatment during the Mössbauer effect measurement (for about 7 h) above T_{x1} still leads to a small but not negligible increase of the CR phase by about 5%, even though the nanocrystalline sample was actually prepared by annealing at higher temperature for 1 h. From figure 9 in [37] one can see that after about 10 min of annealing at temperature higher than T_{x1} the rapid grain growth is already saturated, reaching a value between 8 and 10 nm. The presence of a very small slope in the grain size dependence on the time of annealing results in further small but obviously not negligible grain growth especially for long annealing times. Therefore in order to reach saturation in the nanocrystalline growth in isothermal annealing, an adequate time duration of the annealing process has to be chosen.

The nanocrystallite growth due to diffusion of iron atoms leads to changes in the chemical composition of the amorphous remainder above T_{x1}. The relative concentration of mainly Zr atoms in the amorphous matrix increases, which is manifested in more negative values IS_{AM} as seen from figure 5(b). In addition, a trend of B_{AM} growing, as shown in figure 5(a), is also caused by the increasing contribution of nanocrystallites, implying higher exchange coupling forces among them that are mediated through the amorphous retained phase [38, 39].

Above T_{x2} (931 K), the onset of the second crystallization is evidenced from RT Mössbauer spectra in figures 4(f)–(h). Fe_3Zr crystals featuring hyperfine parameters $IS = -0.05(3)$ mm s^{-1} and $B_{hf} = 24.0(2)$ T appear, which is in agreement with other works [2, 29, 33]. At the same time, remarkable changes in IS_{IF} occur as shown in figure 5(b). Results from HREM reveal the presence of Zr-rich regions in front of the growing interfaces of the α-Fe particles suggesting control of the nanograin growth by Zr diffusion [30]. The same effects are reported in [8].

6. Conclusions

High temperature Mössbauer spectroscopy has been employed to study the temperature dependence of the relationship of microstructure to magnetic properties of ^{57}Fe subsites in $Fe_{90}Zr_7B_3$ NANOPERM-type nanocrystalline alloy at temperatures exceeding that of the second crystallization stage. For this purpose the sample investigated has been prepared by annealing at 893 K for 1 h, which resulted in well developed nanocrystalline structure with average grain size of about 20 nm. Room temperature Mössbauer spectra were subsequently measured after each high temperature step in order to follow temperature induced changes in the sample. The onset of the first $T_{x1} = 782$ K and the second $T_{x2} = 931$ K crystallizations were determined by differential calorimetric scanning performed upon an amorphous precursor. A high statistics Mössbauer spectrum measured for the amorphous ribbon does not confirm

precipitation of nanocrystallites in the as-cast amorphous material. The only appreciable change found in the temperature interval between room temperature and 782 K is the Curie transition of the amorphous component. This magnetic transition is smeared out due to the large amount of nanocrystallites in the sample, which promote the crystalline exchange field penetration through the residual amorphous material, resulting in an enhanced Curie temperature of this phase.

More pronounced changes take place during measurements in the temperature interval between T_{x1} and T_{x2}. Progress of the first crystallization during the Mössbauer experiment at 850 K was detected; this is higher than T_{x1} but still lower than the temperature of the original annealing (893 K).

The room temperature Mössbauer spectra collected after those obtained at temperature higher than T_{x2} have confirmed that the onset of the second crystallization of this ternary alloy is related to precipitation of Fe_3Zr polycrystals which occupy predominantly the interface regions of the nanograins as evidenced by HREM studies.

The consistency of the temperature behaviours of the hyperfine parameters for all three ^{57}Fe components obtained from the fitting model to the Mössbauer spectra of NANOPERM-type ternary alloy through the temperature interval under consideration, supported by the results from earlier low temperature Mössbauer studies and HREM investigations, can be regarded as confirmation of the existence of interfacial regions. This is a step toward the better understanding and description of nanocrystalline alloys prepared by controlled annealing of amorphous precursors.

Acknowledgments

The authors are grateful to Professor G Vogl for continuous support and fruitful discussions and to Professor W Pfeiler for help with the DSC experiments. This work was financed by the Austrian Fonds zur Förderung der Wissenschaftlichen Forschung (FWF) contract No P15421, by the Austrian Federal Ministry for Education, Science and Culture (project GZ 45.529/2-VI/B/7a/2002) and by the VEGA grant No 1/1014/04.

References

[1] Suzuki K, Kataoka N, Inoue A, Makino A and Masumoto T 1990 *Mater. Trans. JIM* **31** 743
[2] Suzuki K, Makino A, Inoue A and Masumoto T 1991 *J. Appl. Phys.* **70** 6232
[3] McHenry M E and Laughlin D E 2000 *Acta Mater.* **48** 223
[4] Nagase T, Umakoshi Y and Sumida N 2002 *Sci. Tech. Adv. Mater.* **3** 119
[5] McHenry M E, Johnson F, Okumura H, Ohkubo T, Ramanan V R V and Laughlin D E 2003 *Scr. Mater.* **48** 881
[6] Kopcewicz M, Idzikowski B and Kalinowska J 2003 *J. Appl. Phys.* **94** 638
[7] Gao Y, Shindo D, Bitoh T and Makino A 2003 *Sci. Tech. Adv. Mater.* **4** 353
[8] Herth S, Rösner H, Rempel A A, Schaefer H E and Würschum R 2003 *Z. Metallk.* **94** 1073
[9] Yoon S H, Kim S B, Lee H M and Kim C h S 2003 *J. Magn. Magn. Mater.* **507** 254
[10] Suzuki K, Cadogan J M, Aoki K and Ringer S P 2003 *J. Magn. Magn. Mater.* **441** 254
[11] Suzuki K, Cadogan J M and Cochrane J W 2003 *Scr. Mater.* **48** 875
[12] Ślawska-Waniewska A and Grenéche J M 1997 *Phys. Rev.* B **56** 8491
[13] Miglierini M and Grenéche J M 1997 *J. Phys.: Condens. Matter* **9** 2321
[14] Suzuki K and Cadogan J M 1998 *Phys. Rev.* B **58** 2730
[15] Grenéche J M, Randrianantoandro N, Ślawska-Waniewska A and Miglierini M 1998 *Hypfine Interact.* **113** 279
[16] Miglierini M and Grenéche J M 1999 *Hyperfine Interact.* **122** 121
[17] Hupe O, Chuev M A, Bremers H, Hesse J and Afanas'ev A M 1999 *J. Phys.: Condens. Matter* **11** 10545
[18] Miglierini M and Grenéche J M 2003 *J. Phys.: Condens. Matter* **15** 5637
[19] Kemény T, Kaptás D, Balogh J, Kiss L F, Pusztai T and Vincze I 1999 *J. Phys.: Condens. Matter* **11** 2841

[20] Balogh J, Bujdosó L, Kaptás D, Kemény T, Vincze I, Szabó S and Beke D L 2000 *Phys. Rev.* B **61** 4109
[21] Kemény T, Kaptás D, Kiss L F, Balogh J, Vincze I, Szabó S and Beke D L 2000 *Hyperfine Interact.* **130** 181
[22] Grenéche J M and Ślawska-Waniewska A 2000 *J. Magn. Magn. Mater.* **215/216** 264
[23] Miglierini M and Grenéche J M 1997 *J. Phys.: Condens. Matter* **9** 2303
[24] Miglierini M and Grenéche J M 1998 *Hyperfine Interact.* **113** 375
[25] Chuev M, Hupe O, Bremers H, Hesse J and Afanas'ev A M 2000 *Hyperfine Interact.* **126** 407
[26] Ciurzyńska W H, Varga L K, Olszewski J, Zbroszczyk J and Hasiak M 2000 *J. Magn. Magn. Mater.* **208** 61
[27] Garitaonandia J S, Gorria P, Fernández Barquín L and Barandiarán J M 2000 *Phys. Rev.* B **61** 6151
[28] Hono K, Zhang Y, Inoue A and Saskurai T 1997 *Mater. Sci. Eng.* A **226–228** 498
[29] Xiong X Y, Finlayson T R and Muddle B C 2001 *Mater. Phys. Mech.* **4** 34
[30] Ohkubo T, Kai H, Makino A and Hirotsu Y 2001 *Mater. Sci. Eng.* A **312** 274
[31] Lagarec K and Rancourt D G 1997 *Nucl. Instrum. Methods Phys. Res.* B **129** 266
[32] Puerta J and Martin P 1981 *Appl. Opt.* **20** 3923
[33] Zhang Y, Hono K, Inoue A, Makino A and Sakurai T 1996 *Acta Mater.* **44** 1497
[34] Kai H, Ohkubo T, Hirotsu Y and Makino A 1999 *Proc. Int. Conf. On Solid-Solid Phase Transformations. '99 (JIMIC-3)* ed M Koiwa, K Otsuka and T Miyazaki, The Japan Institute of Metals, p 1223
[35] Lécaudé N, Perron J C, Randrianantoandro N and Grenéche J M 1999 *Mater. Sci. Forum* **312–314** 487
[36] McHenry M E, Johnson F, Okumura H, Ohkubo T, Ramanan V R V and Laughlin D E 2003 *Scr. Mater.* **48** 881
[37] Garitaonandia J S, Schmool D S and Barandiarán J M 1998 *Phys. Rev.* B **58** 12147
[38] Hernando A and Kulik T 1994 *Phys. Rev.* B **49** 7064
[39] Navarro I, Ortuno M and Hernando A 1996 *Phys. Rev.* B **53** 11656